Dalton Transactions

Accepted Manuscript

ROYAL SOCIETY OF CHEMISTRY

www.rsc.org/dalton

Shape controlled synthesis of hierarchical nickel sulfide by the hydrothermal method

R. Karthikeyan[a], M. Navaneethan[b], J. Archana[b], D. Thangaraju[b], M. Arivanandhan[b] and Y. Hayakawa [a,b,]*

[a]Graduate School of Science and Technology, Shizuoka University, 3-5-1, Johoku, Naka-ku, Hamamatsu, Shizuoka 432-8011, Japan

[b]Research Institute of Electronics, Shizuoka University, 3-5-1, Johoku, Naka-ku, Hamamatsu, Shizuoka 432-8011, Japan

*Corresponding author. Tel/Fax: +81 53 478-1310

E-mail: royhaya@ipc.shizuoka.ac.jp (Y. Hayakawa)

Abstract

Hierarchical structures of nickel sulfide have been grown by the hydrothermal method. Nickel nitrate hexahydrate and thiourea were used as precursor materials to synthesize nickel sulfide. Ethylenediaminetetraaceticacid was used as a capping agent to achieve monodispersity. The different phases of nickel sulfide and its dependency on the precursor concentration were analyzed by X-ray diffractometry. Transmission electron microscopy analysis was used to confirm the phase changes and morphological behavior of the synthesized material. The morphological evolution of the hierarchical structure formation was studied systematically by scanning electron microscopy. In this study, we explore a novel method to control the synthesis of nickel sulfide hierarchical structures by varying the precursor concentration. The two mixed phases enhanced the catalytic activity in the 4-nitro phenol reduction reaction.

Keywords: Nickel sulfide, Hydrothermal method, Hierarchical structures, Phase transformation.

1. Introduction

Nanomaterial properties are dependent on size, shape, and dimensionality[1]. Metal sulfide nanomaterials have attracted significant attention because of their excellent properties and promising applications in electronic and optoelectronic devices. Nickel sulfide is of importance in the metal sulfide family[2–5] because of the variety in its phases and diversity in applications such as in lithium ion batteries[6], supercapacitors[7], and dye-sensitized solar cells[8]. The relatively complex nickel sulfide system was first investigated by Kullard and Yard in 1962[9] . The nickel sulfide system contains a number of phases including NiS_2, Ni_3S_4, Ni_7S_6, Ni_9S_8, α- $Ni_{3+x}S_2$, Ni_3S_2, NiS, and NiS_2[10]. Most of the phases are present at low temperature, which is one of the major advantages for nickel sulfide as a next generation material. According to the phase diagram of nickel sulfide, the sulfur-rich part of the system appears to be rather simple with only a few phases compared with the complex Ni-rich phases. In recent years, many research groups have attempted to prepare different nickel sulfide phases for specific applications. Many researchers have reported that the hexagonal nickel monosulfide (NiS) phase undergoes a metal-to-insulator transition at low temperature (~265 K)[11–14]. When the Ni_3S_4 phase was grown on N-doped graphene, it showed a high electrolytic resistance compared with other nickel sulfide phases [15] and was ferrimagnetic in nature [16]. Ohtani et al. investigated the importance of Ni deficiency on the formation of nickel sulfide which leads to a non-stoichiometric form of $Ni_{1-x}S$[17]. It

is challenging to synthesize nickel sulfide by the low-temperature chemical route with controlled phases from complex source materials.

Apart from the structural focus on nickel sulfide, several nickel sulfide nanostructure morphologies, such as nanorods, nanotubes, nanowires, nanosheets, nanoprisms, layered structures[18], flower-like[10], and ball-like hollow spheres have been reported on. Higher nanostructure (or microstructure) dimensions that compose the building blocks in hierarchical morphologies have shown potential use in many fields including gas sensing[19] and catalytic applications. Weiquan cai et.al reported the structure transformation of Boehmite by mediating the sulfate under hydrothermal conditions to achieve morphologies from nanoflakes to hollow microspheres[20]. The synthesis of nickel sulfide hierarchical structures has been reported previously by several research groups[21,22]. Li et al. discussed the formation of β-NiS flower-like architectures in the presence of the citrate anion as a capping agent at various growth temperatures[10]. Wang et al. explained the effect of temperature on the formation of NiS_2 spherical cuboids[17]. Several other researchers have explained the hierarchical structure formation of nickel sulfide; however structural changes with respect to the concentration and formation of hierarchical morphologies by the hydrothermal method have not yet been investigated. Ethylenediaminetetraaceticacid (EDTA) is a well-known chelating agent and crystal growth modifier. However, nickel sulfide synthesis using EDTA has not yet been reported on.

In this paper, we report on the synthesis of nickel sulfide hierarchical structures with EDTA as a capping agent using nickel nitrate hexahydrate ($Ni(NO_3)_2 \cdot 6H_2O$) and thiourea (CH_4N_2S) as precursors in the hydrothermal method. EDTA was chosen as capping agent because of its good anionic interaction with metal

sulfides and control of morphology[23–25]. The effect of precursor material concentration (i.e. $Ni(NO_3)_2 \cdot 6H_2O$, CH_4N_2S, and EDTA) on the formation mechanism of nickel sulfide hierarchical structures and phase control were investigated.

2. Experimental

2.1 Synthesis procedures

All reagents (analytical-grade purity) were purchased from Wako Chemicals, Japan and were used without further purification. To synthesize the nickel sulfide hierarchical structures, 1 mol CH_4N_2S was added to a 5 mol L^{-1} $Ni(NO_3)_2 \cdot 6H_2O$ solution. EDTA (0.2 mol) was added as a capping agent under vigorous stirring. Experiments were carried out with and without EDTA addition. EDTA addition resulted in a solution color change from dark green to a pale-blue with an increased solution viscosity. The precursor material concentration is abbreviated as A (0.5 mol $Ni(NO_3)_2 \cdot 6H_2O$, 1 mol CH_4N_2S and 0.2 mol EDTA). A mixture of these materials was stirred continuously for 60 min, and the solution was then transferred to a 0.1 L Teflon-lined autoclave for hydrothermal reaction at 160°C for 10 h. The nickel sulfide precipitate was then filtered, washed with distilled water three times and dried at 60°C. To understand the formation mechanism of the hierarchical structures, low concentrations of precursor materials, such as A/10 and A/5, were prepared under identical conditions. These synthesized materials were collected and dried at the same temperature. All other conditions (100 mL distilled water, 160°C reaction temperature, and 10 h reaction time) were kept constant. To avoid the possibility of coordination of the S^{2-} anion with the nickel complex and the formation of more complex phases, the reaction temperature was fixed at 160°C.

2.2 Characterization

The product crystal structure was characterized by powder X-ray diffraction (XRD) with a scan rate of 0.04° s^{-1} in the 2θ range from 10 to 80° using a Rigaku (Japan) X-ray diffractometer (RINT-2200, CuKα radiation, λ =1.54178 Å). Field emission scanning electron microscope (FESEM) images were taken with a JEOL JSM 6320F instrument to observe sample surface morphology. High resolution transmission electron microscope (HRTEM) images were recorded using a JEOL JEM 2100F microscope at an accelerating voltage of 200 kV. Quantitative analysis was conducted by X-ray photoelectron spectroscopy (XPS) using a Shimadzu ESCA 3100 spectrophotometer.

3. Results and discussion

3.1 Effect of EDTA

When the reaction was carried out in water, the sulfur to nickel molar ratio (S:Ni) was maintained at 2:1 in all experiments. Fig. 1 (a) and (b) show the FESEM images of samples prepared with the 0.5 mol nickel source and the 1 mol sulfur source concentrations, where (a) is EDTA-uncapped and (b) is EDTA-capped nickel sulfide. The EDTA-uncapped nickel sulfide particles consist of improper hierarchical morphologies hundreds of nanometers to several micrometers in size. The EDTA-capped sample contains sheets composed of ball-like structures. Addition of the EDTA anion controlled the reaction between the sulfur and nickel ions, and resulted in the formation of monodispersed hierarchical structures. The addition of EDTA to the Ni^{2+} solution produced a Ni^{2+} complex and slowed down the effect of CH_4N_2S during the reaction[26].

3.2 Effect of precursor concentrations

To understand the formation mechanism of hierarchical ball-like structures with respect to the phase changes, further experiments were carried out with different precursor material concentrations such as A/5 and A/10. Table 1 shows details of the phases present in the synthesized products with respect to concentration. At the lower A/10 concentration, the nickel source was fixed at 0.05 mol, the sulfur source at 0.1 mol and the EDTA capping agent at 0.02 mol. A typical XRD pattern of the as-prepared nickel sulfide samples is shown in Fig. 2. All the diffraction peaks of the A/10 sample were well matched with the Joint Committee on Powder Diffraction Standards (JCPDS) card number 01-075-0613 for the NiS_2 and 03-065-3419 for the NiS phase.

For the A/5 concentration, a large change was observed in the XRD pattern. A phase transformation was observed from NiS to $Ni_{17}S_{18}$, which can be seen from a shift in the dominant peak positions from 30.06°, 34.55°, and 45.73° to 30.16°, 34.62°, and 45.70°, respectively (see Fig. 2). Along with the $Ni_{17}S_{18}$, a NiS_2 phase also appeared and matched the JCPDS card number 01-089-3058 closely. A further increase in concentration (A) resulted in a phase change from NiS_2 to Ni_3S_4. The new Ni_3S_4 phase matched the JCPDS card number 01-076-1813 closely.

Figures 3 (a)–(f) and 4 (a)–(f) show the FESEM and TEM images, respectively, of the nickel sulfide samples with different precursor concentrations (a and b) A/10, (c and d) A/5 and (e and f) A. For the A/10 concentration, the product was composed of cubic and rod-like structures, which were nanometers to hundreds of nanometers in size. The TEM images support the observation of mixed morphologies of cubic and rod-like structures as shown in Fig. 4 (a). The 2.5 Å interplanar spacing

matched the distance between the crystal plane of (210) of the NiS_2 phase as mentioned in Fig. 4 (b). The corresponding Fast-Fourier-Transform (FFT) pattern showed that the synthesized product was crystalline.

When the concentration was increased to A/5, the product was flower-like with a few cubic structures as shown in Fig. 3 (c). As can be seen from Fig 4 (d), nanosheet-like structures were arranged in flower-like architectures for the sample with A/5 concentrations. Figure 4 (e) and (f) are the TEM and HRTEM images, respectively, of the A/5 sample. The TEM images indicate the presence of cubic- and hexagonal-shaped nanocrystals and the HRTEM images show that the product is crystalline. The interplanar spacing of 3.4 Å corresponds to the NiS_2 (111) phase. These results are in agreement with the XRD results and show that the product morphology is affected significantly by concentration. The TEM results confirm the mixed NiS sample phase. At the A concentration, monodispersed hierarchical morphology was observed as shown in Fig. 3 (e) and (f). The monodispersed hierarchical structures were composed of nanosheets and the ball –like structures were composed of cubic nanoparticles. The average sheets composed hierarchical diameter was 6–8 μm and cube constructed balls diameter was 3–4 μm. Figure 4 (e) and (f) show the TEM and HRTEM images of the A sample. The interplanar distance of 2.3 Å matched the (400) crystalline plane of cubic Ni_3S_4 closely. The clear lattice fringes and FFT pattern confirmed the quality of the prepared materials.

Figure 5 (a) and (b) show the XPS patterns of nickel sulfide prepared from different precursor concentrations of A/10, A/5, and A. The doublet peaks at 162.5 and 169.2 eV (Fig. 5 (a)) correspond to the S $2p_{3/2}$ and $2p_{1/2}$ binding energies, and agree closely with literature values[27]. The doublet peaks of S 2p indicate the presence of

mono- and polysulfide for all concentrations tested. Two distinct peaks at 853 and 870 eV correspond to the $2p_{3/2}$ and $2p_{1/2}$ states of Ni in nickel sulfide, respectively[8,28]. The absence of a satellite region of 856 eV at the A concentration supports the fact that there was no nickel sulfate peak ($NiSO_4$)[29].

3.3 Effect of sulfur source concentration

To understand the importance of thiourea as a sulfur source, different experiments were carried out by fixing the nickel source concentration as 0.50 mol and capping agent concentration as 0.20 mol. Sulfur source was varied as 0.50, 0.75 and 1.0 mol. Fig. 6 and Fig. 7 show the XRD patterns and FESEM images of samples with different sulfur source concentrations. When the concentration was fixed as 1:1 ratio of sulfur to nickel ions, it resulted in the formation of two different phases of nickel sulfide (NiS_2 and Ni_3S_4). When the sulfur concentration was increased to 0.75 mol, reaction between the nickel-EDTA complex and sulfur was increased. This resulted in the appearance of new phase of $Ni_{17}S_{18}$. Presence of more sulfur ions was favored to react with more number of nickel ions, which resulted the formation of $Ni_{17}S_{18}$ phase with sheet-like morphology as observed in the FESEM images (fig. 7 (b)). Further increase in the concentration of sulfur with the nickel to sulfur ratio 1:2, stable phases of nickel sulfide ($Ni_{17}S_{18}$ and Ni_3S_4) with thick sheets composed hierarchy morphologies were formed. Fig.8 (a) and (b) show the HRTEM images of different sulfur source concentrations. In Fig. 8(a), the interplanar distance of 2.9 Å was well matched with the (311) peak of Ni_3S_4 phase, similarly, interplanar distance of 2.6 Å from Fig.8 (b) was well matched with the (244) peak of Ni_3S_4 phase.

Catalytic activity of nickel sulfide catalysts for the reduction of 4-nitrophenol

The catalytic property of the synthesized nickel sulfide architectures was

evaluated by employing the reduction of 4-nitrophenol into 4-aminophenol[30,31]. During the reaction, active hydrogen species are firstly transferred to the surface of synthesized products and then the reduction of 4-nitrophenol was taken place by the reaction of adsorbed 4-nitro phenol molecules. The kinetic process was monitored by UV-vis spectroscopy measurements. Fig.9 shows the absorbance spectra of 4-nitro phenol and the catalytic reduction with the nickel sulfide products such as A, A/5 and A/10. The absorbance peak at 400 nm was directly associated with the concentration of 4-nitrophenolate ions. Absorbance nature of the catalyst was added and the samples were measured as a function of time. The addition of A/10 and A/5 resulted in a steady decrease in the concentration of 4-nitrophenolate ions in solution as seen in the absorbance spectra. The sample A showed complete disappearance of Abs_{400nm} compared to the other sample A/10 and A/5 (see Fig.9 inset). In addition, the appearance of new peak at 293 nm was confirmed the formation of 4-aminophenol. All the catalytic reaction was observed with 4-NP for the period of 3 min. The above results clearly demonstrated that the existence of the phases of Ni_3S_4 and $Ni_{17}S_{18}$ greatly enhanced the catalytic property.

Mechanism of hierarchical structures evolution:

Fig.10 (a) and (b) shows the schematics of reaction mechanism and growth process of different nickel sulfide architectures. At the A/10 concentration, the limited availability of nickel and sulfur ions in the precursor solution resulted in simple and near stoichiometric phases of NiS_2 and NiS. Further increase in the concentration of source material in A/5 increased the availability of more molecules for reaction, which leads to the formation of different sulfur-rich phases as shown in Fig. 2. The rod-like morphology was changed to sheet-like morphology due to the addition of source

materials. The add-atoms growth was taken place on the rods and thus the morphology was changed. Further increase of source material (A), the morphology of the sample eventually changed to three dimensional hierarchical structures (Fig. 3 (e) and (f)). This is mainly due to the Oswald ripening mechanism[10]. The high concentration of precursor solution resulted in the formation of different phases of nickel sulfide (Ni_3S_4 and $Ni_{17}S_{18}$) confirmed by XRD analysis (Fig. 2).

From the catalytic activity of the nickel sulfide catalysts, the reduction ability of sample A was better than the samples A/5 and A/10. Sample A was consisted of two different phases of Ni_3S_4 and $Ni_{17}S_{18}$. N. Mahmood et.al, demonstrated the importance of Ni_3S_4 as a catalytic material for the application of lithium ion batteries[15]. $Ni_{17}S_{18}$ was a pure metallic phase with the advantage of having two different catalytic phases in a synthesized product A, therefore the activity was enhanced. The sample A/5 and A/10 consisted of semiconducting phase of NiS_2 along with NiS.

From the different sulfur source concentrations, it is well understood that all different higher concentrations were feasible to form hierarchical architectures. However, amount of sulfur concentration played significant role in the formation of building blocks. When the amount of sulfur concentration was very less or equal ratio of sulfur to nickel ions, reaction between the nickel EDTA complex and sulfur anion was dominant for the formation of Ni_3S_4. A small quantity of NiS_2 was also retained with Ni_3S_4 phases. When the amount of sulfur source was increased to 0.75 mol, thin-sheets composed hierarchical structures ($Ni_{17}S_{18}$) were formed with cube constructed balls (Ni_3S_4). Further the ratio of nickel to sulfur ions of 1:2 resulted in the thick sheets composed balls with cube composed architectures. The experimental results demonstrate that the precursor concentration plays a significant role in the

formation of hierarchical structures and different nickel sulfide phases.

4. Conclusion

Monodisperse nickel sulfide hierarchical structures were synthesized by the hydrothermal method. The effect of EDTA capping agent and different concentrations of source materials on the phase, morphology, and stoichiometric ratio were investigated. The addition of an EDTA capping agent resulted in uniform size and morphology. Different precursor material concentrations of A/10, A/5, and A were used to observe the phase changes in the synthesized products. Morphological phase change behavior was studied using FESEM and TEM analysis. Flower- and ball-like sheet architectures were visible. A significant change in the nickel sulfide phases was observed with respect to source material concentration by XRD analysis. The sulfur-rich Ni_3S_4 and $Ni_{17}S_{18}$ phases consisted of two different hierarchical structures which enhanced the catalytic activity.

Acknowledgements

The authors would like to thank Mr. T. Koyama and Mr. Tomada for their support in the XRD, FESEM and XPS analysis. R. Karthikeyan thanks MEXT-Japan for the award of a research fellowship.

References

1. J. E. Murphy, M. C. Beard, A. G. Norman, S. P. Ahrenkiel, J. C. Johnson, P. Yu, O. I. Mićić, R. J. Ellingson, and A. J. Nozik, *J. Am. Chem. Soc.*, 2006, **128**, 3241–7.

2. R. D. Tilley and D. a. Jefferson, *J. Phys. Chem. B*, 2002, **106**, 10895–10901.

3. P. Nguyen, H. T. Ng, T. Yamada, M. K. Smith, J. Li, J. Han, and M. Meyyappan, 2004.

4. Y.-D. Li, H.-W. Liao, Y. Ding, Y.-T. Qian, L. Yang, and G.-E. Zhou, *Chem. Mater.*, 1998, **10**, 2301–2303.

5. K. Q. Peng, Z. P. Huang, and J. Zhu, *Adv. Mater.*, 2004, **16**, 73–76.

6. L. Mi, Q. Ding, W. Chen, L. Zhao, H. Hou, C. Liu, C. Shen, and Z. Zheng, *Dalton Trans.*, 2013, **42**, 5724–30.

7. T. Zhu, H. Bin Wu, Y. Wang, R. Xu, and X. W. D. Lou, *Adv. Energy Mater.*, 2012, **2**, 1497–1502.

8. W. S. Chi, J. W. Han, S. Yang, D. K. Roh, H. Lee, and J. H. Kim, *Chem. Commun. (Camb).*, 2012, **48**, 9501–3.

9. G. Kullerud and R. a. Yund, *J. Petrol.*, 1962, **3**, 126–175.

10. and Y. Q. Haibo Li, Lanlan Chai, Xiaoqing Wang, Xueying Wu, Guangcheng Xi, yankuan Liu, *J. Cryst. Growth Des.*, 2007, **7**, 1918–1922.

11. J. T. Sparks and T. Komoto, *J. Appl. Phys.*, 1963, **34**, 1191.

12. J. Sparks and T. Komoto, *Phys. Lett.*, 1967, **25**, 5–6.

13. J. Sparks and T. Komoto, *Rev. Mod. Phys.*, 1968, **40**.

14. J. and J. P. R. A. S. Barker, *Phys. Rev. B*, 1974, **10**, 987–994.

15. N. Mahmood, C. Zhang, and Y. Hou, *Small*, 2013, **9**, 1321–8.

16. A. Manthiram and Y. U. Jeong, 1999, **681**, 679–681.

17. T. Ohtani, *J. Phys. Soc. Japan*, 1974, **37**, 701–710.

18. X. Jiang, Y. Xie, J. Lu, L. Zhu, W. He, and Y. Qian, *Adv. Mater.*, 2001, **13**, 1278.

19. J.-H. Lee, *Sensors Actuators B Chem.*, 2009, **140**, 319–336.

20. W. Cai, J. Yu, S. Gu, and M. Jaroniec, *Cryst. Growth Des.*, 2010, **10**, 3977–3982.

21. L. Wang, Y. Zhu, H. Li, Q. Li, and Y. Qian, *J. Solid State Chem.*, 2010, **183**, 223–227.

22. S. Ni, G. Zhou, X. Wang, X. Sun, F. Yang, Y. Liu, and D. He, *Mater. Chem. Phys.*, 2010, **120**, 426–430.

23. D. A. Reddy, G. Murali, R. P. Vijayalakshmi, and B. K. Reddy, *Appl. Phys. A*, 2011, **105**, 119–124.

24. S. Mondal and S. Verma, *Zeitschrift für Anorg. und Allg. Chemie*, 2014, n/a–n/a.

25. S. Gnanam and V. Rajendran, 2013, **17**, 185–190.

26. Z. Meng, Y. Peng, W. Yu, and Y. Qian, *Mater. Chem. Phys.*, 2002, **74**, 230–233.

27. S. Krishnakumar and D. Sarma, *Phys. Rev. B*, 2003, **68**, 155110.

28. H. W. Nesbitt, D. Legrand, and G. M. Bancroft, *Phys. Chem. Miner.*, 2000, **27**, 357–366.

29. D. A. L. Legrand, H. W. A. N. Esbitt, and G. M. I. B. Ancroft, 1998, **83**, 1256–1265.

30. J. Zhang, G. Chen, M. Chaker, F. Rosei, and D. Ma, *Appl. Catal. B Environ.*, 2013, **132-133**, 107–115.

31. T. Yu, J. Zeng, B. Lim, and Y. Xia, *Adv. Mater.*, 2010, **22**, 5188–92.

Table 1 Phases observed with different experimental conditions.

Different concentrations of precursor materials $Ni(NO_3)_2.6H_2O$: CH_4N_2S : EDTA	Phases from XRD analysis
A/10 (0.05 mol : 0.1 mol : 0.02 mol)	NiS (03-065-3419) NiS_2 (01-075-0613)
A/5 (0.1 mol : 0.2 mol : 0.04 mol)	$Ni_{17}S_{18}$ (01-089-3058) NiS_2 (01-075-0613)
A (0.5 mol : 1.0 mol : 0.2 mmol)	$Ni_{17}S_{18}$ (01-089-3058) Ni_3S_4 (01-076-1813)

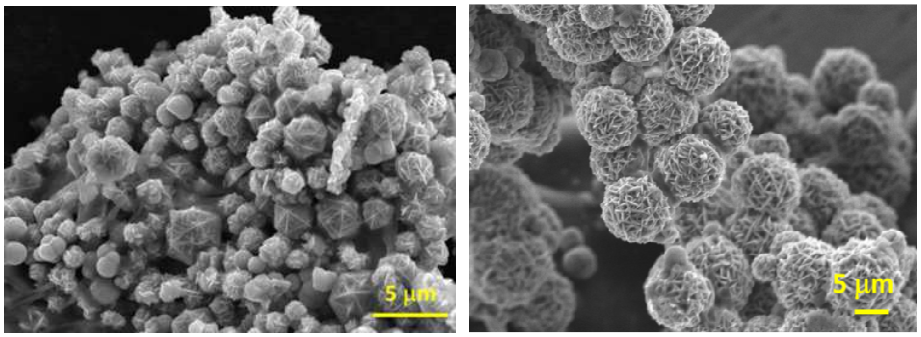

(a) **(b)**

Fig. 1 FESEM images of (a) EDTA-uncapped (b) EDTA-capped nickel sulfide samples.

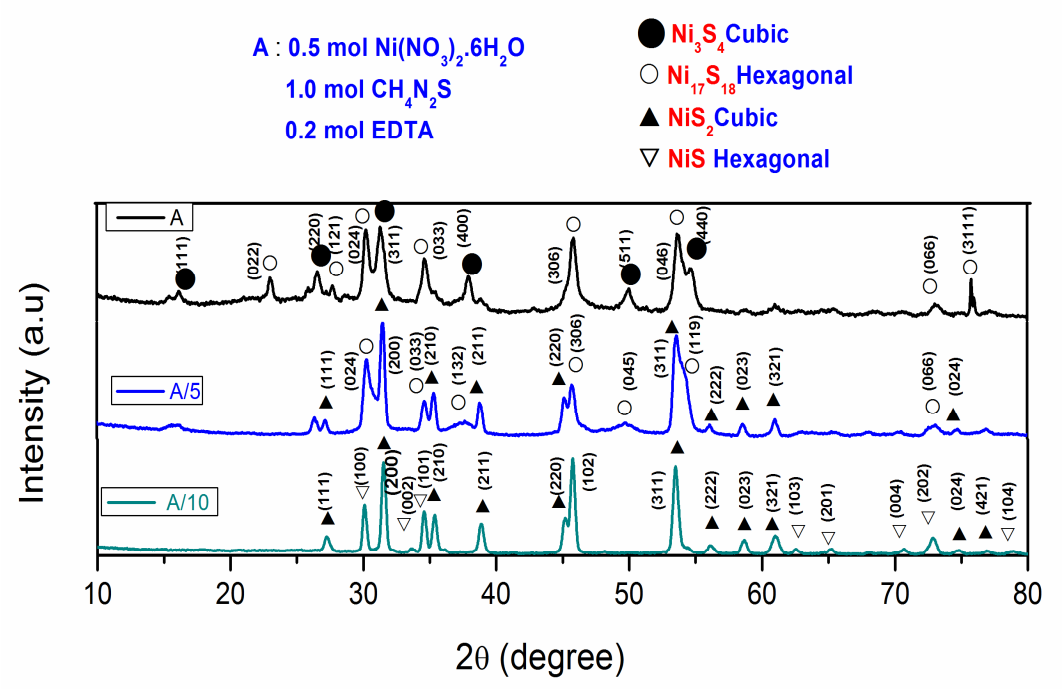

Fig. 2 XRD patterns for different stoichiometric precursor material concentrations.

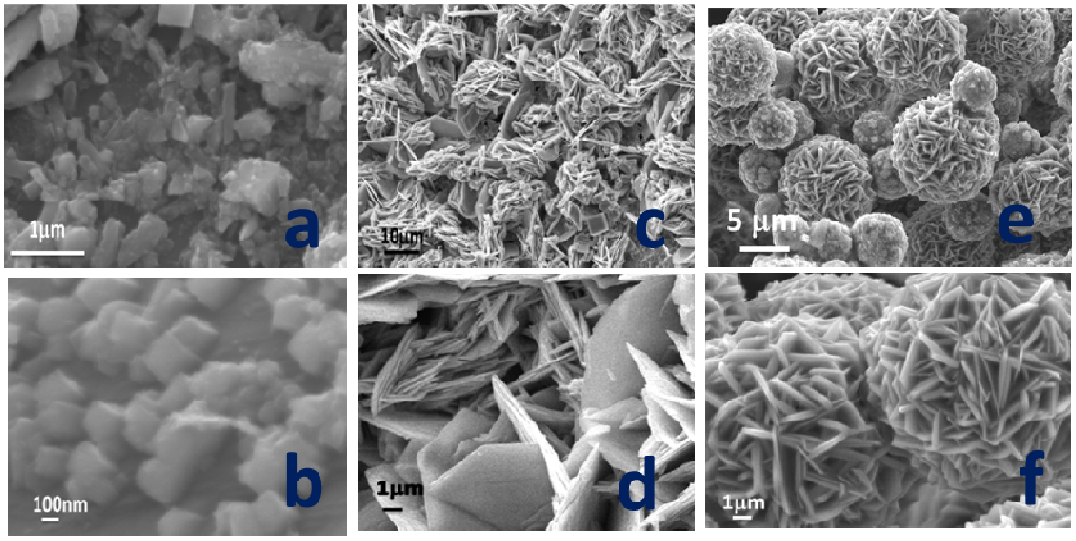

Fig. 3 FESEM images for (a,b) A/10, (c,d) A/5, and (e,f) A source material concentrations.

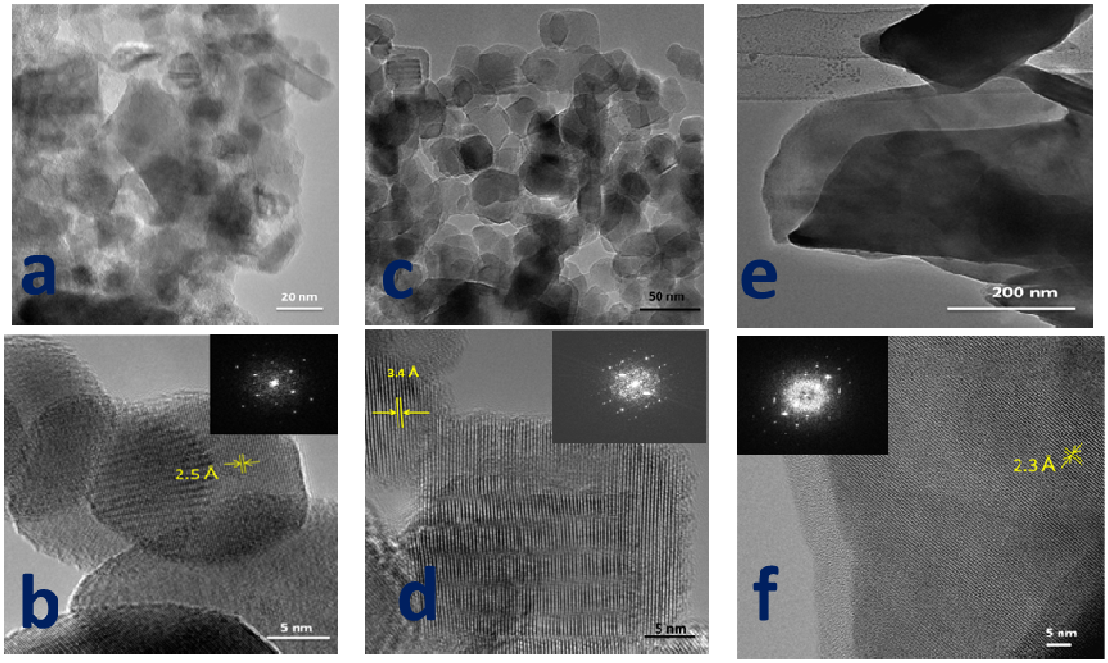

Fig. 4 TEM and HRTEM images for (a,b) A/10, (c,d) A/5, and (e,f) A source material concentrations.

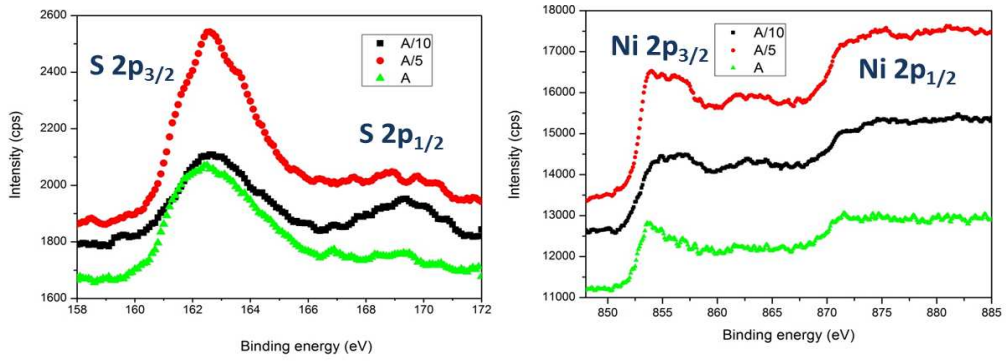

(a) (b)

Fig. 5 XPS spectra of nickel sulfides after Ar ion etching: (a) S and (b) Ni peaks.

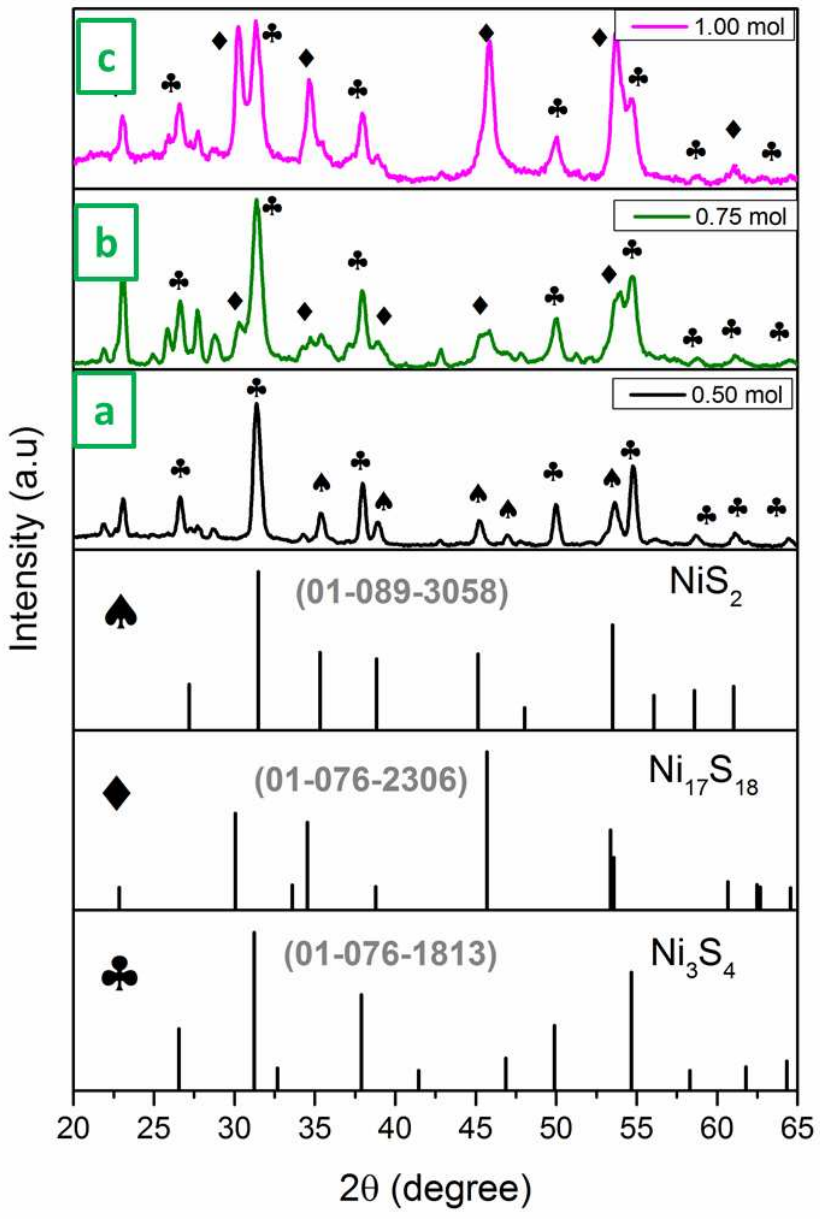

Fig. 6 XRD patterns for different sulfur source concentrations a) 0.50 mol b) 0.75 mol and c) 1.00 mol.

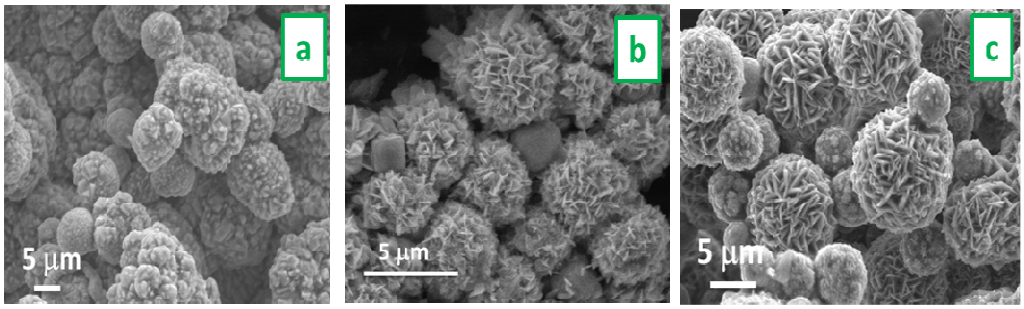

Fig. 7 FESEM images a) 0.50 mol b) 0.75 mol and c) 1.00 mol of sulfur source concentrations.

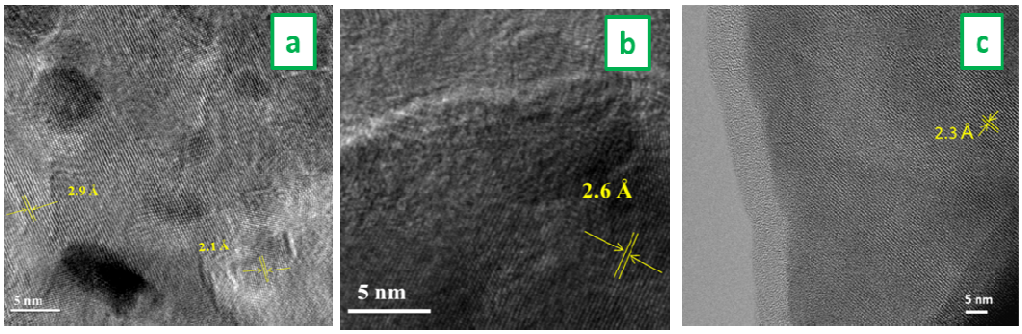

Fig. 8 HRTEM images a) 0.50 mol b) 0.75 mol and c) 1.00 mol of sulfur source concentrations.

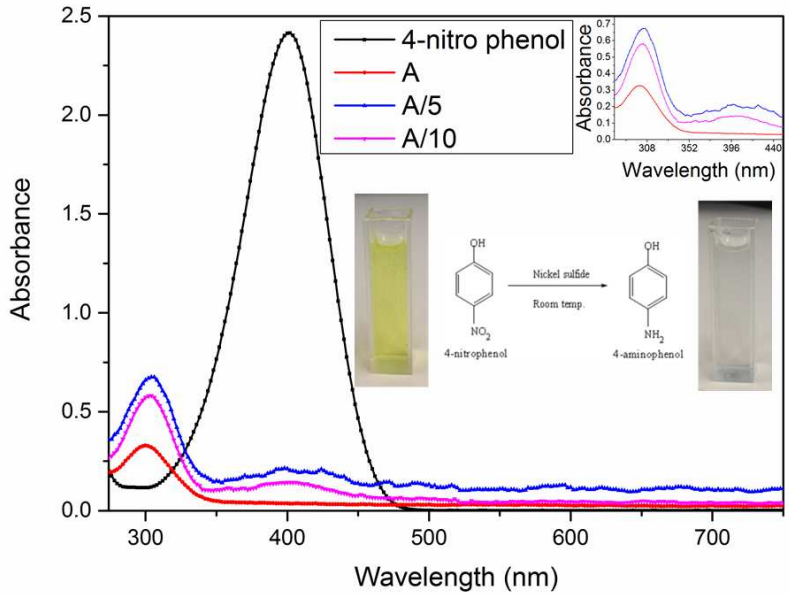

Fig. 9 UV-vis spectrum of reduction of 4-NP using nickel sulfide architectures.

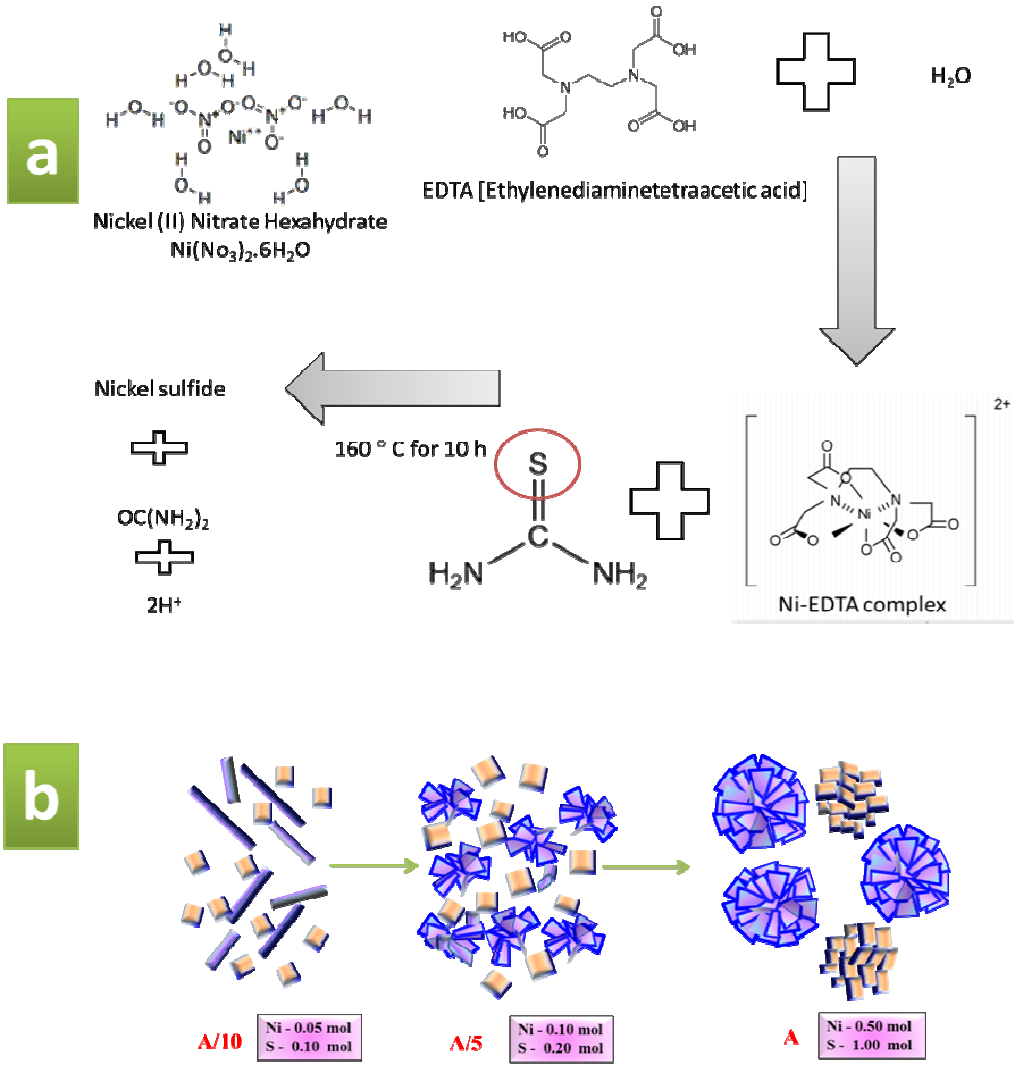

Fig. 10 Schematics of (a) reaction mechanism and (b) growth process of different nickel sulfide architectures